Carbon-supported Platinum Electrocatalysts probed in a Gas Diffusion Setup with Alkaline Environment: how Particle Size and Mesoscopic Environment influence the Degradation Mechanism

Shima Alinejad[a], Jonathan Quinson[b], Johanna Schröder[a], Jacob J. K. Kirkensgaard[c], Matthias Arenz[a*]

[a] Department of Chemistry and Biochemistry, University of Bern, Freiestrasse 3, 3012 Bern, Switzerland

[b] Department of Chemistry, University of Copenhagen, Universitetsparken 5, 2100 Copenhagen Ø, Denmark

[c] Department of Food Science, University of Copenhagen, Rolighedsvej 26, 1958 Frederiksberg, Denmark

*Corresponding author

University of Bern, Freiestrasse 3, CH-3012 Bern, Switzerland

Phone: +41 31 631 53 84

Email: matthias.arenz@dcb.unibe.ch

Graphical Abstract

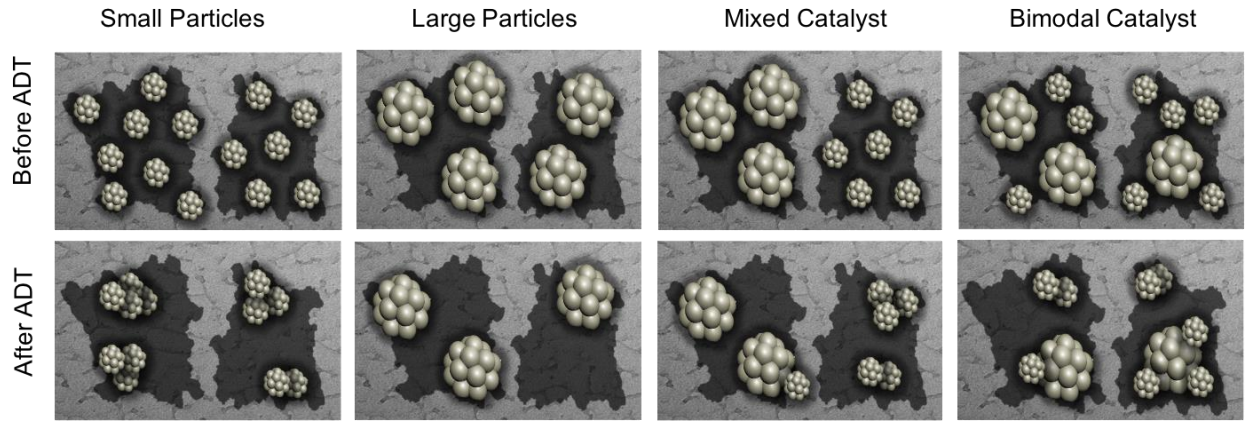

Abstract

In recent years, extensive research has been performed concerning the stability of fuel cell catalysts in acidic environment. By comparison, only few studies address the degradation mechanism(s) of fuel cell catalysts in alkaline media. In this work, we investigate the stability of four different types of Pt/C fuel cell catalysts upon applying accelerated degradation tests (ADTs) in a gas diffusion electrode (GDE) setup equipped with an anion exchange membrane (AEM). In contrast to previous investigations exposing the catalysts to liquid electrolyte, the GDE setup provides a realistic three-phase boundary of the reactant gas, catalyst and ionomer which enables reactant transport rates close to real fuel cells. Therefore, the GDE setup mimics the degradation of the catalyst under more realistic reaction conditions as compared to conventional electrochemical cells. Combining the determination of the loss in electrochemically active surface area (ECSA) of the Pt/C catalysts via CO stripping measurements with the change in particle size distribution determined by small-angle X-ray scattering (SAXS) measurements, we demonstrate that i) the degradation mechanism depends on the investigated Pt/C catalyst and might indeed be different to the one observed in conventional electrochemical cells, ii) degradation is increased in an oxygen gas atmosphere (as compared to an inert atmosphere), and iii) the observed degradation mechanism depends on the mesoscopic environment of the active phase. The measurements indicate an increased particle growth if small and large particles are immobilized next to each other on the same carbon support flakes as compared to a simple mix of two catalysts with small and large particles, respectively.

KEYWORDS: Pt/C fuel cell catalysts; accelerated degradation test; alkaline media; small-angle X-ray scattering

1. Introduction

Fuel cell technology stands on the brink of large-scale commercialization. However, although commercial fuel cell products have been introduced, they face the challenges of durability and cost[1,2]. Despite the fact that most automotive applications target the use of proton exchange membrane fuel cells (PEMFC) powered with hydrogen, in recent years anion exchange membrane fuel cells (AEMFC)[3,4] have received increasing attention as well. The advantages of AEMFCs as compared to PEMFCs are i) "faster" oxygen reduction reaction (ORR) kinetics, ii) a broader choice of catalyst materials, in particular platinum-group-metal (PGM) and non-PGM catalysts, iii) enabling a wide range of fuel options in addition to pure hydrogen, and iv) a more comprehensive range of polymer chemistries[5,6]. Despite these advantages, durability is a key issue for the application of AEMFCs. It has been reported for both PGM[5,7,8] and non-PGM[9] electrodes that the durability of electrodes in liquid hydroxide electrolytes is limited. These reports challenge the common belief for AEMFCs that alkaline media can prevent the degradation of the electrode materials[10,11]. For example, Zadick et al.[7] reported severe degradation of Pt/C electrocatalysts, demonstrating a significant loss in electrochemically active surface area (ECSA) during potential excursions between 0.1 V_{RHE} and 1.2 V_{RHE} in aqueous electrolyte. Employing identical location transmission electron microscopy (IL-TEM)[12], the authors show that the observed degradation is mainly due to the detachment of the Pt nanoparticles (NPs) from the carbon support.

In the present work, we investigate the degradation of Pt/C catalysts in alkaline conditions under more realistic reaction conditions as compared to conventional electrochemical cells where the catalyst is exposed to an aqueous electrolyte. Instead, a gas diffusion electrode (GDE) setup[13–15] is employed, which has been used recently to study the stability of carbon-supported platinum catalysts in acidic media[16]. To obtain alkaline conditions, for the present study the Nafion membrane from a PEMFC has been replaced with an anion exchange membrane (AEM) and an alkaline ionomer was mixed into the catalyst layer. In order to stress the catalysts, an accelerated degradation test (ADT) protocol simulating load-cycles is implemented that consists of stepping the applied electrode potential between 0.6 and 1.0 $V_{RHE,}$ which was recommended by the Fuel Cell Commercialization Conference of Japan (FCCJ)[17,18]. The catalyst degradation is investigated by a combination of CO stripping measurements to establish the loss in ECSA and the characterization of the catalysts by small-angle X-ray scattering (SAXS) to establish the particle

size distribution in the catalyst layer. In contrast to IL-TEM, SAXS is an integral method which probes changes in the entire catalyst layer before and after performing the ADT[19,20].

2. Experimental

2.1. Chemicals, materials, and gases

Ultrapure Milli-Q water (resistivity > 18.2 MΩ cm, total organic carbon (TOC) < 5 ppb) from a Milli-Q system (Millipore) was used for the electrolyte preparation, the catalyst ink formulation, the membrane activation, and the GDE cell cleaning. In addition to the Milli-Q water, for the preparation of the catalyst ink formulation isopropanol (IPA, 99.7+%, Alfa Aesar), commercial Pt/C catalysts (TEC10E20A, 19.4 wt. % Pt, TEC10E50E-HT, 50.6 wt. % Pt, from Tanaka Kikinzoku Kogyo), and an alkaline ionomer (Sustainion® XA-9 Alkaline Ionomer 5% in ethanol, Dioxide Materials) were used. Potassium hydroxide (KOH, Merck) was used for the electrolyte preparation. An AEM (Sustainion® X37-50 Grade RT Membrane, with a dry thickness of 50 µm thick, Dioxide Materials) and gas diffusion layers (GDL) with a microporous layer (MPL) (Sigracet 39BC, 325 µm thick, Fuel Cell Store) and without a microporous layer (Sigracet 39AA, 280 µm thick, Fuel Cell Store) were employed in the GDE cell measurements. Ar (99.999%), O_2 (99.999 %), and CO (99.97%) from Air Liquide were used in the electrochemical measurements.

2.2. Gas diffusion electrode setup

An in-house developed gas diffusion electrode setup (Figure 1) was employed in all electrochemical measurements[13,14,16]. The working electrode (WE) in form of a GDE was placed on top of the flow field in the stainless steel cell body and an activated AEM was pressed on top of the GDE to separate the liquid electrolyte from the catalyst layer and create more realistic conditions. The upper cell part above the anion membrane is made of polytetrafluoroethylene (PTFE). A reversible hydrogen electrode (RHE) and a platinum wire were used as a reference electrode (RE) and a counter electrode (CE), respectively. In order to improve the reproducibility of the measurements, the CE was placed inside a glass capillary with a glass frit on the bottom to avoid the trapping of gas bubbles in the Teflon cell. All potentials in this study are referred to the RHE potential. For cleaning, the Teflon upper part was soaked in mixed acid (H_2SO_4 : HNO_3 = 1 :1, v:v) overnight. Subsequently, it was rinsed thoroughly by Milli-Q water and boiled in Milli-Q water twice. Before each measurement, the Teflon upper part, RE, CE, and the glass capillary

were boiled once in Milli-Q water, followed by rinsing thoroughly by Milli-Q water. The CE was annealed after rinsing with Milli-Q water.

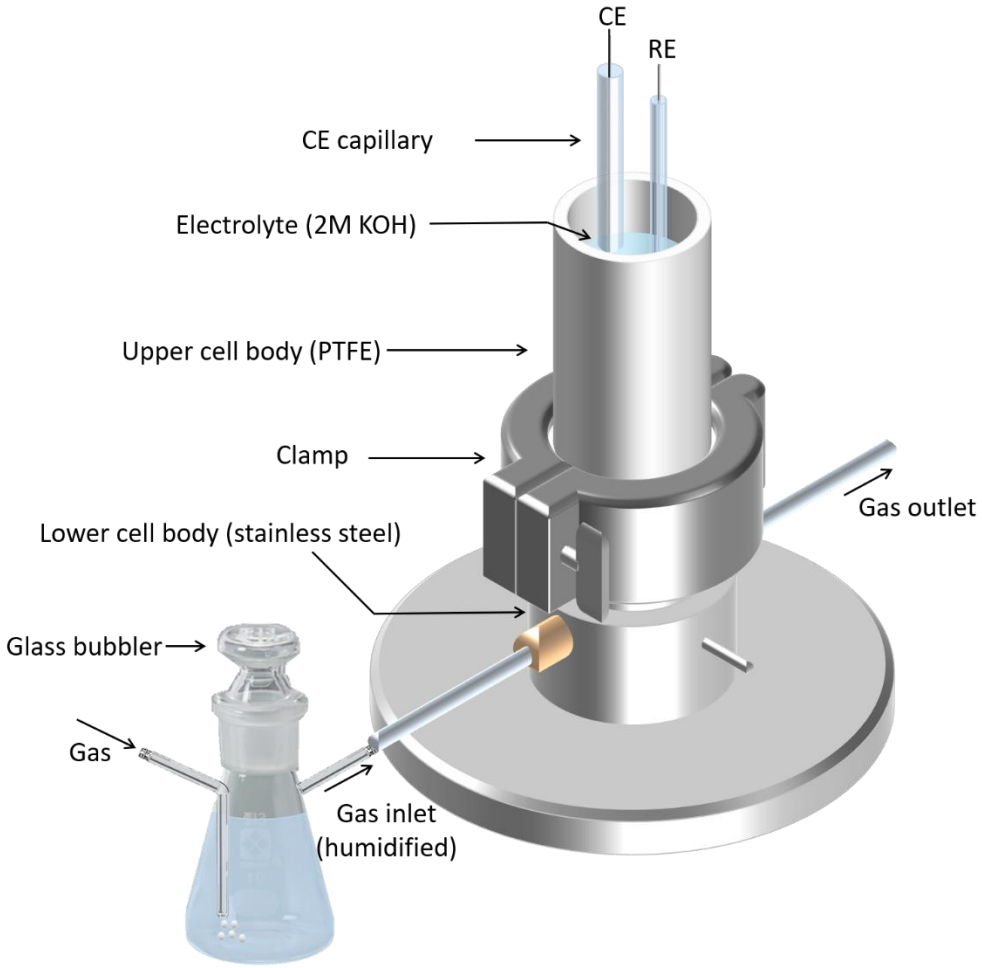

Figure 1. Sketch of the GDE cell employed in the present study. The upper cell body is pressed to the lower cell body by a clamp. A glass bubbler is connected to the gas inlet to humidify the gas.

2.3. Pt/C catalysts and catalyst ink formulation

Four different Pt/C catalysts were used in this work (Table 1). The first two (i.e. TEC10E20A and TEC10E50E-HT) are commercial catalysts and exhibit only one narrow size range of Pt nanoparticles. In the following we address these two catalysts as monomodal and name them according to their average particle size as 1-2 nm and 4-5 nm Pt/C[21]. To obtain an ink of these two catalysts, the respective catalyst powder was dispersed in a mixture of Milli-Q water : IPA (1:3; v:v) to obtain for each catalyst 20 mL of ink with a Pt concentration of 0.1 mg mL^{-1}. The anion

ionomer was added to obtain a mass ratio of ionomer:carbon (1:1). Thereafter the glass vials with the catalyst inks were placed in an ultrasonic bath and sonicated for 15 min.

The other two types of Pt/C catalyst were composed of two NP populations with distinguishable particle size distributions, i.e. 1-2 nm and 4-5 nm. The first catalyst was obtained by simply mixing the two commercial catalysts, 1-2 nm and 4-5 nm Pt/C in a Pt mass ratio of 1:1 in the ink formulation. Hereafter we refer to this catalyst as "mixed" catalyst. In this catalyst, the closest neighbor for a 'small' and 'large' NP is a NP of the same (similar) size. For the preparation of the catalyst that we refer to in the following as "bimodal" catalyst, the two populations were obtained by depositing ca. 4 nm Pt NPs onto the commercial 1-2 nm Pt/C catalyst. The Pt NPs were prepared by a surfactant-free and size-controlled colloidal synthesis in alkaline ethylene glycol with NaOH/Pt molar ratio of 5 leading to an expected particle size of ca. 4 nm[22]. The as-prepared Pt NPs were then immobilized on the 1-2 nm Pt/C catalyst with a Pt mass ratio of 4:6 (1-2 nm Pt/C : ~4 nm Pt NPs). In this catalyst, there is a similar likelihood that 'small' and 'large' NPs are nearest neighbors as there is that NPs with the same size are nearest neighbors. For both catalysts, i.e. mixed and bimodal, the same procedure as above was used for the ink preparation leading to 20 mL of ink with a Pt concentration of 0.1 mg mL^{-1}.

Table 1. Particle size of four different Pt/C catalysts, which were used in this work.

Pt/C catalyst	Mean Particle size based on TEM	Name in this work
TEC10E20A	1-2 nm[21]	1-2 nm Pt/C
TEC10E50E-HT	4-5 nm[21]	4-5 nm Pt/C
Mix of 1:1 ratio TEC10E20A and TEC10E50E-HT	1-2 nm : 4-5 nm	Mixed
Homemade bimodal Pt/C catalyst	1-2 nm Pt/C : ~4 nm[22] Pt NPs	Bimodal

2.4. Working electrode preparation

To prepare the catalyst films, a cylindrical reservoir with a cross-sectional area of 10.75 cm^2 was placed on top of the gas diffusion layer (GDL) with an MPL (Sigracet 39BC), which was positioned onto a sand core filter. All this was placed on a collecting bottle, as described by Yarlagadda et al.[23]. The reservoir was filled with 20 mL of ink and a vacuum was applied with the help of a water jet pump. By sucking the ink through the GDL a homogenous catalyst layer was obtained, which was dried overnight in air. The resulting Pt loading on the GDE was 0.2 mg_{Pt} cm^{-}

$^{2}_{geo}$ which is in the typical range for fuel cell applications[24]. A circle of Ø 3 mm was punched from this GDE to prepare the WE with the help of a hydraulic press. For the pressing, a Teflon sheet, a GDL without MPL (Ø 2 cm), a GDL with MPL (Ø 2 cm) with a hole of Ø 3 mm in the center that was filled with the punched Ø 3 mm GDE, and an anion membrane, respectively, were placed between two Teflon blocks. The two Teflon blocks were then pressed together for 10 min at 2 tons pressure. Before use, the anion membrane was activated in 1 M KOH, and thereafter punched into circles with a diameter of 2 cm for the pressing. The punched membranes were kept in 1 M KOH and thoroughly rinsed with Ultrapure Milli-Q water before assembling into the GDE cell. Several combinations of different types of membranes and electrolytes and their influence on ECSA determination are detailed in Table S1.

2.5. Electrochemical measurements

All electrochemical measurements were performed at ambient temperature using a computer-controlled potentiostat (ECi 242, NordicElectrochemistry). The upper cell compartment of the GDE setup was filled with 2 M KOH aqueous solution. Before the measurements, the WE was purged with humidified Ar gas through the inlet of the GDE setup. The gas was humidified with the help of a glass bubbler filled with Milli-Q water. Before starting the measurements, the catalyst layer was cleaned by potential cycling between 0.06 and 1.10 V_{RHE} until a stable cyclic voltammogram could be observed (ca. 10 cycles at a scan rate of 50 mV s^{-1} and 15 cycles at a scan rate of 500 mV s^{-1}). The resistance between the working electrode (WE) and RE (ca. 18 Ω) was compensated to around 2 Ω by using the analog positive feedback scheme of the potentiostat. The residual resistance was determined online using an AC signal (5 kHz, 5 mV)[25]. An ADT protocol was applied to simulate load-cycle conditions[16] stepping the applied electrode potential between 0.6 and 1.0 V_{RHE} with a holding time of 3 seconds at each potential. 1000 and 2000 of these steps were applied in Ar and O_2 atmosphere. A representative example of the current densities recorded during the ADT in Ar and O_2 atmosphere is shown in Figure S1. The ECSA of the catalyst was determined before and after the ADT by conducting CO stripping voltammetry. The CV recorded in Ar gas was subtracted as background and a baseline correction between the chosen peak limits was performed to avoid any influence of capacitive currents from the carbon support. An example of the procedure performed in a standard electrochemical cell with acidic electrolyte is shown in an instructional video journal[26]. The CO stripping was performed by purging CO gas for 5 min while holding potential at 0.05 V_{RHE} and thereafter Ar for an additional 5 min. The ECSA was

determined from the CO oxidation charge (Q_{CO}) recorded at a scan rate of 50 mV s^{-1} assuming an oxidation charge of 390 µC cm^{-2}_{Pt} and taking into account the Pt loading of 0.2 mg_{Pt} cm^{-2}_{geo}[26].

2.1. SAXS analysis

SAXS measurements were performed at the Niels Bohr Institute, University of Copenhagen, Denmark on a SAXSLab instrument equipped with a 100XL+ micro-focus sealed X-ray tube (Rigaku), producing a photon beam with a wavelength of 1.54 Å. For recording the scattering patterns, a 2D 300 K Pilatus detector (Dectris) was used. The two-dimensional scattering data were azimuthally averaged, normalized by the incident radiation intensity, the sample exposure time and the transmission. Using SAXGUI reduction software[27], data were then corrected for background and detector inhomogeneities. The samples consisting of the NPs on the GDL were sealed between two 5–7 µm thick mica windows and measurements performed in vacuum. The background measurement was made with a GDL Sigracet 39BC without any NPs. For each catalyst at least two samples were analyzed by SAXS before and after applying the ADT. The results from all SAXS measurements are listed in the supporting information (SI) in TableS2.

The radially averaged intensity I(q) is expressed as a function of the scattering vector $q = 4\pi\cdot\sin(\theta)/\lambda$, where λ is the wavelength, and 2θ is the scattering angle. The background-corrected scattering data were fitted using a power law to take into account the behavior at low q value and a model of one or two polydisperse spheres described by a volume-weighted log-normal distribution. The scattering data are fitted to the following expression:

$$I(q)= A\cdot q^{-n} + C_1\cdot\int P_{s1}(q,R)V_1(R)D_1(R)dR + C_2\cdot\int P_{s2}(q,R)V_2(R)D_2(R)dR$$

where $A\cdot q^{-n}$ corresponds to the power law where A and n are free parameters, C_1 and C_2 are scaling constants, Ps_1 and Ps_2 the sphere form factors, V_1 and V_2 the particle volumes and D_1 and D_2 the log-normal size distribution. The sphere form factor is given by: [28,29]

$$Ps(q,R)=\left(3\,\frac{\sin(qR)-qR\cos(qR)}{(qR)^3}\right)^2$$

and the log-normal distribution by:

$$D(R)=\frac{1}{R\sigma\sqrt{2\pi}}\exp\left(\frac{-\left[\ln\left(\frac{R}{R_0}\right)\right]^2}{2\sigma^2}\right)$$

where σ is the variance and R_0 the geometric mean of the log-normal distribution. The fitting was done using home written MATLAB code.

The free parameters in the model are A, n, C_1, R_1, σ_1, C_2, R_2, σ_2. The values obtained for these parameters are reported in Table S2. In order to account for the two populations, the reported probability density functions were weighted by the relative surface contribution of the spheres as detailed in the SI. The scattering data and corresponding fits are reported in Figure S4. In one case, see Table S2, a hard-sphere structure factor F(R,η) described in Reference[30] was added to improve the fit.

3. Results and discussion

The aim of this work is to investigate the stability of different Pt/C fuel cell catalysts in an alkaline environment under more realistic reaction conditions as compared to previous studies using conventional electrochemical cells. For this, we employed our recently developed GDE setup[13–15], which was previously used to mimic the environment of proton exchange membrane fuel cells (PEMFCs) in ADT studies[16] and adjusted the conditions of AEMFCs.

3.1. ECSA determination in alkaline environment via CO stripping

In degradation studies, evaluating the change in ECSA is of central importance. Considering suitable methods for the ECSA determination, it is important to ascertain that the effect of the ECSA determination itself is negligible in comparison with the effect of the degradation protocol. CO adsorption and oxidation, i.e. CO stripping, is the standard method for the ECSA determination in acidic environment[31,32]. In aqueous alkaline electrolyte, CO stripping is sometimes avoided to prevent carbonate formation as well as to avoid additional degradation induced by the CO oxidation reaction. Instead, a transfer between alkaline and acidic aqueous electrolyte can be performed[7]. As such a "change in environment" is not feasible in the GDE setup, at first, we scrutinized the influence of CO stripping on the catalyst stability. In Figure 2, the effect of CO stripping employed in the GDE setup in an alkaline environment is summarized for the 4-5 nm Pt/C catalyst. 10 consecutive CO stripping tests were performed and a total surface area loss of 6 % was recorded from the first CO stripping test (dark blue) to the last one (light red). It is therefore concluded that individual (single) CO stripping measurements have indeed negligible influence on the catalyst degradation in the GDE setup. Hence in the following, CO stripping was employed to determine the ECSA at the beginning and the end of the ADT. Furthermore, this result

indicates that particle detachment due to carbonate formation, see discussion below, is not significant in the GDE setup and thus alkaline fuel cells not containing liquid electrolyte.

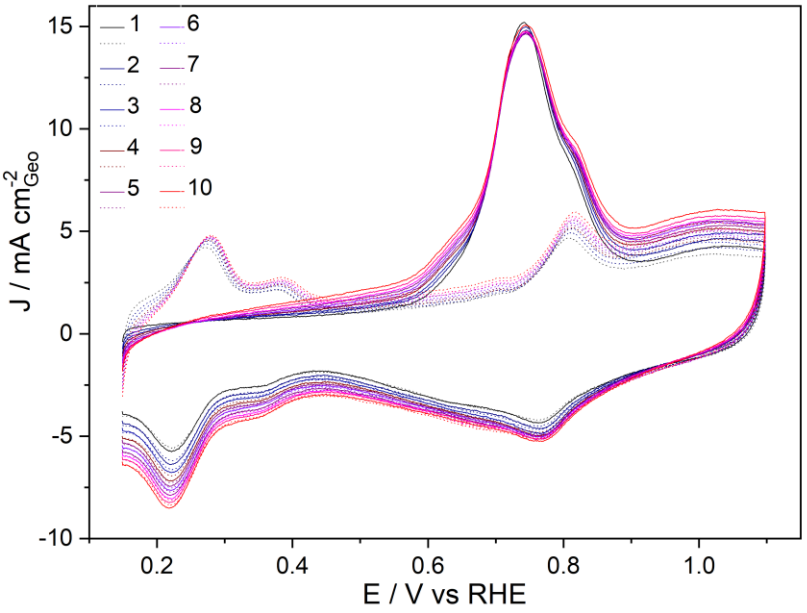

Figure 2. Representative CO stripping curves (solid lines) and subsequent cyclic voltammograms in Ar (dashed lines) of 4-5 nm Pt/C (TEC10E50E-HT). During the CO purging, the potential was held at 0.05 V_{RHE} for 5 min. All measurements were performed at room temperature.

3.2. Comparison of different Pt/C catalysts for ADT measurements under an Ar atmosphere

From the different ADT protocols discussed in the literature[33], we chose for this work a protocol simulating load-cycles, which is a popular approach suggested by the fuel cell commercialization conference of Japan (FCCJ)[17,34]. In addition, the suitability of the load-cycle protocol for monitoring the catalyst degradation in the GDE setup was demonstrated in our previous work[16]. In this ADT protocol, the applied electrode potential is stepped between 0.6 and 1.0 V_{RHE} holding the potential for three seconds at each potential. The lower potential limit (0.6 V_{RHE}) simulates a full load condition, whereas the high potential limit (1.0 V_{RHE}) is close to the open circuit potential of Pt and simulates the cell voltage under idle conditions. As mentioned above, the degradation is monitored by CO stripping experiments before and after the ADT protocol to determine the total loss of ECSA.

In Figure 3, representative CO stripping curves and subsequent cyclic voltammograms recorded in inert environment (purging with Ar gas) are shown for the different Pt/C catalysts. The plot compares the measurements before and after 1000 steps of the load-cycle ADT protocol applied

under Ar atmosphere. In Table 2, the corresponding initial ECSA of these Pt/C catalysts and their ECSA loss applying the load-cycle ADT protocol in Ar and O_2 atmosphere, respectively, are summarized. We performed 1000 and 2000 steps of the load-cycle protocol in Ar atmosphere, whereas due to the increased degradation, see also discussion below, in O_2 atmosphere only 1000 steps were performed. TEM micrographs of the two monomodal commercial Pt/C catalyst powders, 1-2 nm and 4-5 nm Pt/C were shown in our previous work[16,21].

The CVs display the typical features of Pt with hydrogen underpotential deposition (H_{upd}), double layer region, and Pt oxidation and reduction in the potential range of 0.15-1.10 V_{RHE}. Also the CO stripping curves are similar to their counterparts recorded in conventional electrochemical cells[35]. Furthermore, it is noticed that the determined ECSA of the pristine Pt/C catalysts is smaller than their ECSA measured in acidic media[21]. The same observation has been made previously[35], but was not discussed in detail. As always, a similar difference in ECSA between acid and alkaline environment is observed, we link this difference to different CO coverages in the two media. The different absolute ECSA values in alkaline and acid environment, however, do not influence the conclusions drawn in this work.

Applying the ADT protocol, the results obtained in alkaline environment indicate a significantly higher ECSA loss for Pt/C as compared to previous GDE measurements in acidic media[16]. This finding is consistent with the reported measurements performed in conventional electrochemical cells, where the results of ADT were directly compared for acidic and alkaline aqueous electrolyte[36]. Furthermore, as expected, the 1-2 nm Pt/C catalyst is significantly less stable than the 4-5 nm Pt/C catalyst. Upon applying 1000 and 2000 steps of the load-cycling protocol in Ar atmosphere its ECSA loss is 71 ± 2 % and 79 ± 1 %, respectively, as compared to 23 ± 2 % and 39 ± 1 % for the 4-5 nm Pt/C catalyst. Note that the stability improvement of the larger particles might not be only due to the larger particle size of the active Pt phase, but also due to the synthesis route and heat treatment method of the commercial catalysts, which are not publicly available.

As expected, the mixed catalyst exhibits an ECSA loss upon applying the ADT protocol that is higher than the loss observed for the 4-5 nm Pt/C and lower than the one of the 1-2 nm Pt/C catalyst. Interestingly, for the bimodal catalyst it is found that despite of the slightly lower initial ECSA as compared to the mixed catalyst, its ECSA loss is consistently larger than the one of the mixed catalyst. Without any further characterization, it is difficult to interpret this finding. It might be the result of different degradation mechanisms for the two catalysts, but this is speculation if

only ECSA losses are considered. Therefore, to obtain a better understanding of the different degradation mechanisms of the individual Pt/C catalysts in alkaline environment, we analyzed the catalyst layers by SAXS[20,37], which is discussed below.

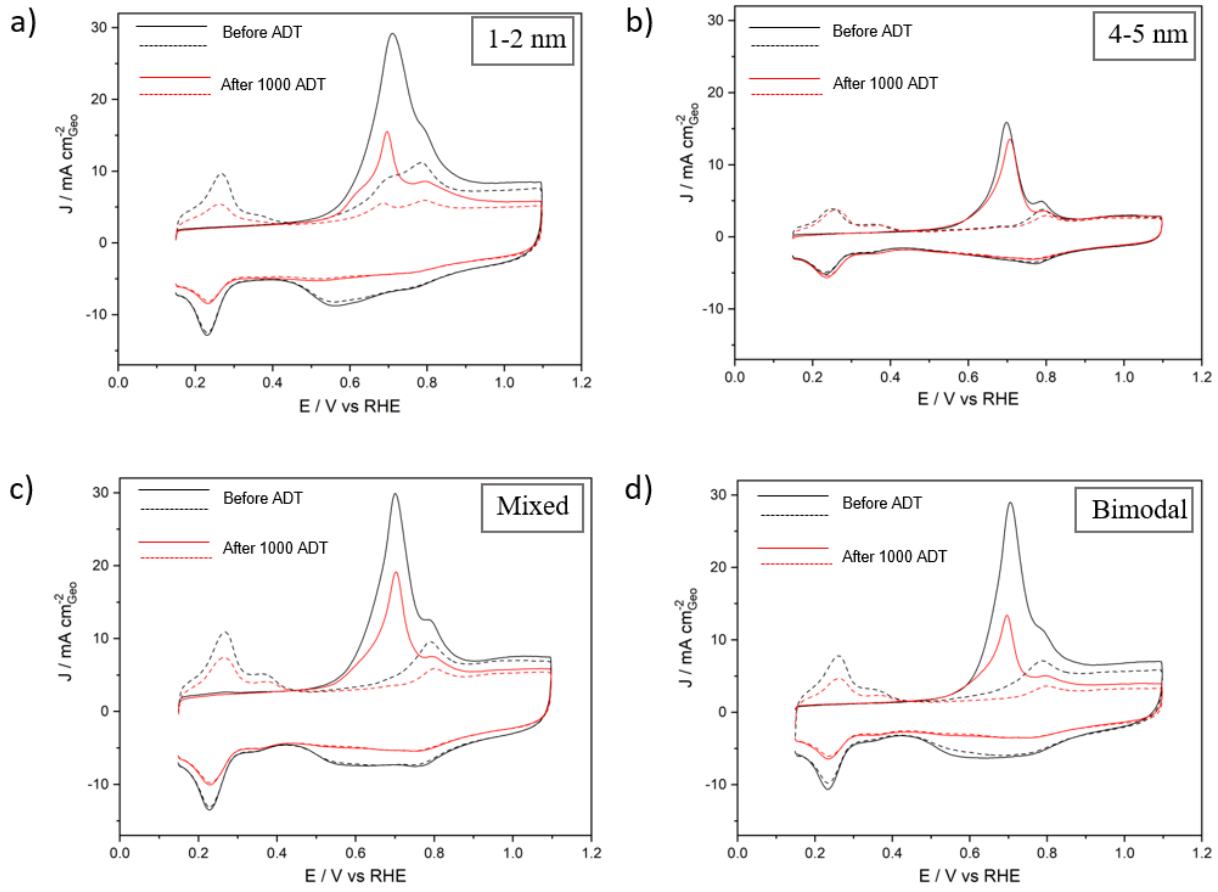

Figure 3. Representative CO stripping curves (solid line) and subsequent cyclic voltammograms in Ar (dashed line) of 1-2 nm (a), 4-5 nm (b), mixed (c), and bimodal (d) Pt/C catalysts before (black lines) and after (red lines) 1000 steps of ADTs in Ar atmosphere. All measurements were performed at room temperature.

Table 2. ECSA loss of different Pt/C catalysts determined by CO stripping. The ADT consisted of 1000 and 2000 steps between 0.6 and 1.0 V_{RHE} in Ar and O_2 atmosphere, respectively. The measurements were conducted at room temperature. All indicated uncertainties are the standard deviation from three measurements.

Pt/C Catalyst	ECSA before ADT ($m^2\ g^{-1}_{Pt}$)	ECSA after ADT ($m^2\ g^{-1}_{Pt}$)		ECSA Loss (%)	
		Ar atmosphere	O_2 atmosphere	Ar atmosphere	O_2 atmosphere

		1000 steps	2000 steps	1000 steps	1000 steps	2000 steps	1000 steps
1-2 nm	70 ± 2	20 ± 2	14 ± 3	11 ± 4	71 ± 2	79 ± 1	84 ± 1
4-5 nm	38 ± 3	30 ± 3	23 ± 2	15 ± 3	23 ± 2	39 ± 1	59 ± 2
Mixed catalyst	63 ± 3	33 ± 3	27 ± 3	20 ± 3	47 ± 1	56 ± 1	67 ± 3
Bimodal catalyst	53 ± 2	22 ± 1	14 ± 2	10 ± 3	58 ± 1	72 ± 2	80 ± 1

3.3. Comparison of different Pt/C catalysts subjected to ADT measurements in an O_2 atmosphere

Before discussing the analysis of the SAXS measurements, we also tested the influence of the gas atmosphere on the resulting ECSA loss. Performing the same ADT protocol for 1000 steps in an O_2 atmosphere instead of an Ar atmosphere leads to a significant decrease in ECSA, see Figure 4 and Table 2. The oxidizing environment of the O_2 gas causes such an increase in degradation that only 1000 steps could be performed. For example, the ECSA loss for the 4-5 nm Pt/C catalyst increases from 23 ± 2 % under Ar atmosphere to 59 ± 2 % under O_2 atmosphere. The trend in stability of the individual catalysts thereby remains the same as the one observed in Ar atmosphere. However, it is important to point out that in previous studies in acidic environment, for the same catalyst (4-5 nm Pt/C) not only a significantly lower ECSA loss was observed but the observed ECSA loss was independent of the reactant gas atmosphere; i.e. ECSA losses of 19 ± 1 % and 18 ± 1 % after 9000 ADT load-cycles were observed under Ar atmosphere and O_2 atmosphere, respectively[16]. The ECSA measurements in acidic and alkaline media were performed under the same conditions. Therefore, it can be concluded that not only the alkaline media is more aggressive than the acidic one, but also that the reactant gas atmosphere influences the observed degradation in a different manner in both environments.

Furthermore, the CO stripping curves after the ADT in the O_2 atmosphere, which are presented in Figure 4, show a tilting or bending which might indicate the presence of O_2 during the recording of the stripping curves. Although the effect is not entirely clear at this point, it might be that some

O_2 is trapped in the membrane or catalyst layer as such tilting was not observed when performing the ADT in Ar atmosphere. The tilting can be reduced by purging the catalyst layer for 30 min with Ar gas before recording the CO stripping curve. However, to have a fair comparison the measurements presented in the Figure 4 were performed in the same manner as for the ADT protocol in Ar atmosphere. Further, it should be noted that the tilting does not cause an error for the CO peak integration as the subsequent cyclic voltammograms in Ar recorded atmosphere are tilted as well.

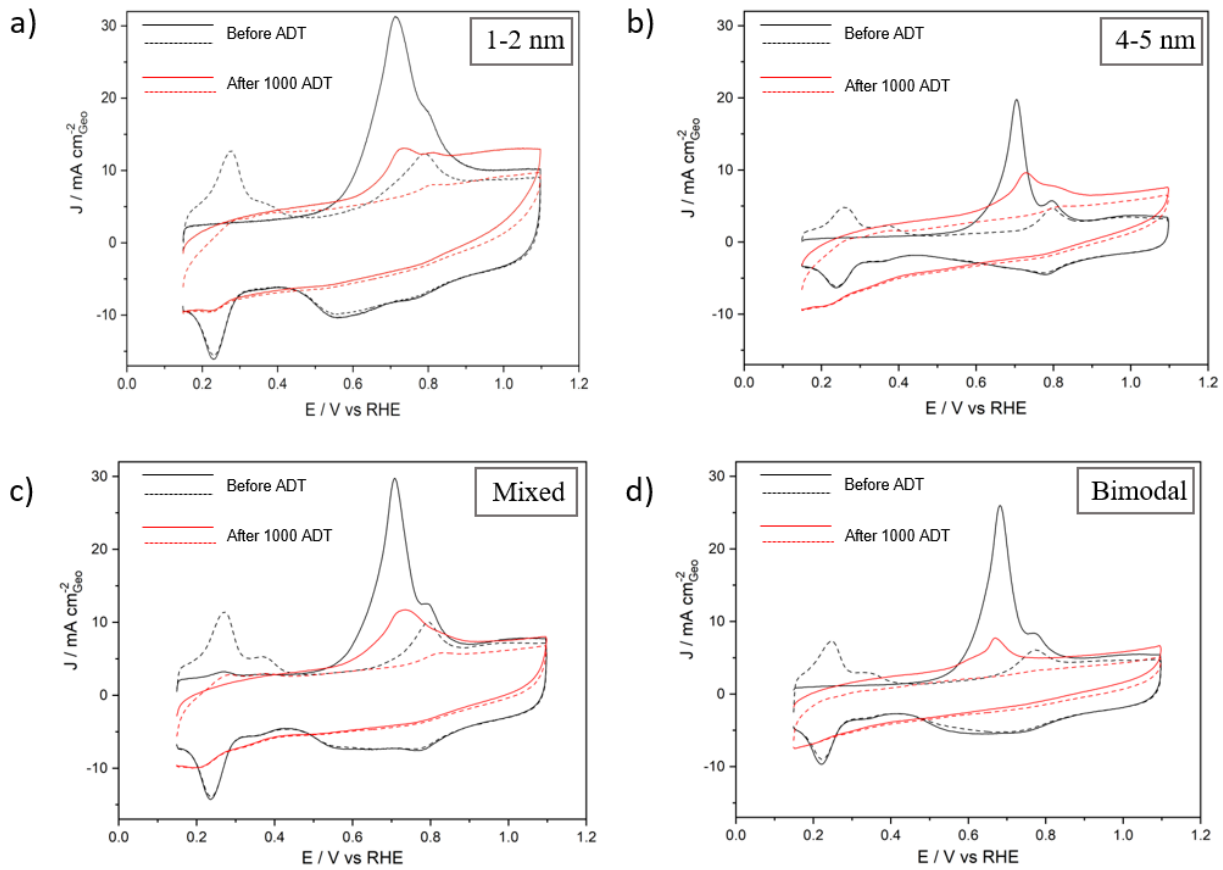

Figure 4. Representative CO stripping curves (solid line) and subsequent cyclic voltammograms in Ar (dashed line) of 1-2 nm (a), 4-5 nm (b), mixed (c), and bimodal (d) Pt/C catalysts before (black lines) and after (red lines) 1000 steps of ADTs in O_2 atmosphere. All measurements were performed at room temperature.

3.4. Elucidating the degradation mechanism with the help of SAXS analysis

In the discussion above, the analysis of the degradation of the different Pt/C catalysts was limited to the change in ECSA. To investigate the degradation mechanism, a physical characterization of the catalysts and its changes is required. The degradation mechanisms of carbon-supported platinum-group-metal electrocatalysts can be divided into four main categories,

migration/coalescence, metal dissolution with and without electrochemical Ostwald ripening, and particle detachment[36,38]. Often these degradation mechanisms are investigated by microscopic methods such as TEM. Here we chose a different approach and employ SAXS. Benefits of a SAXS characterization as compared to TEM investigations are i) that it does not require a disassembly of the catalyst layer and ii) probes the overall changes in a macroscopic volume. The results of the SAXS analysis are summarized in Figure 5 showing the particle size distributions expressed in log-normal plots before and after 2000 steps of the load-cycle ADT in the Ar atmosphere and after 1000 steps of the same ADT protocol in O_2 atmosphere. The derived average particle sizes for all Pt/C catalysts are listed in Table 3. A comparison of the particle size distribution for the 4-5 nm Pt/C catalyst, after 1000 and 2000 steps of the load-cycles ADT in the Ar atmosphere is provided in the SI (Figure S2) demonstrating that there are no significant differences between the two.

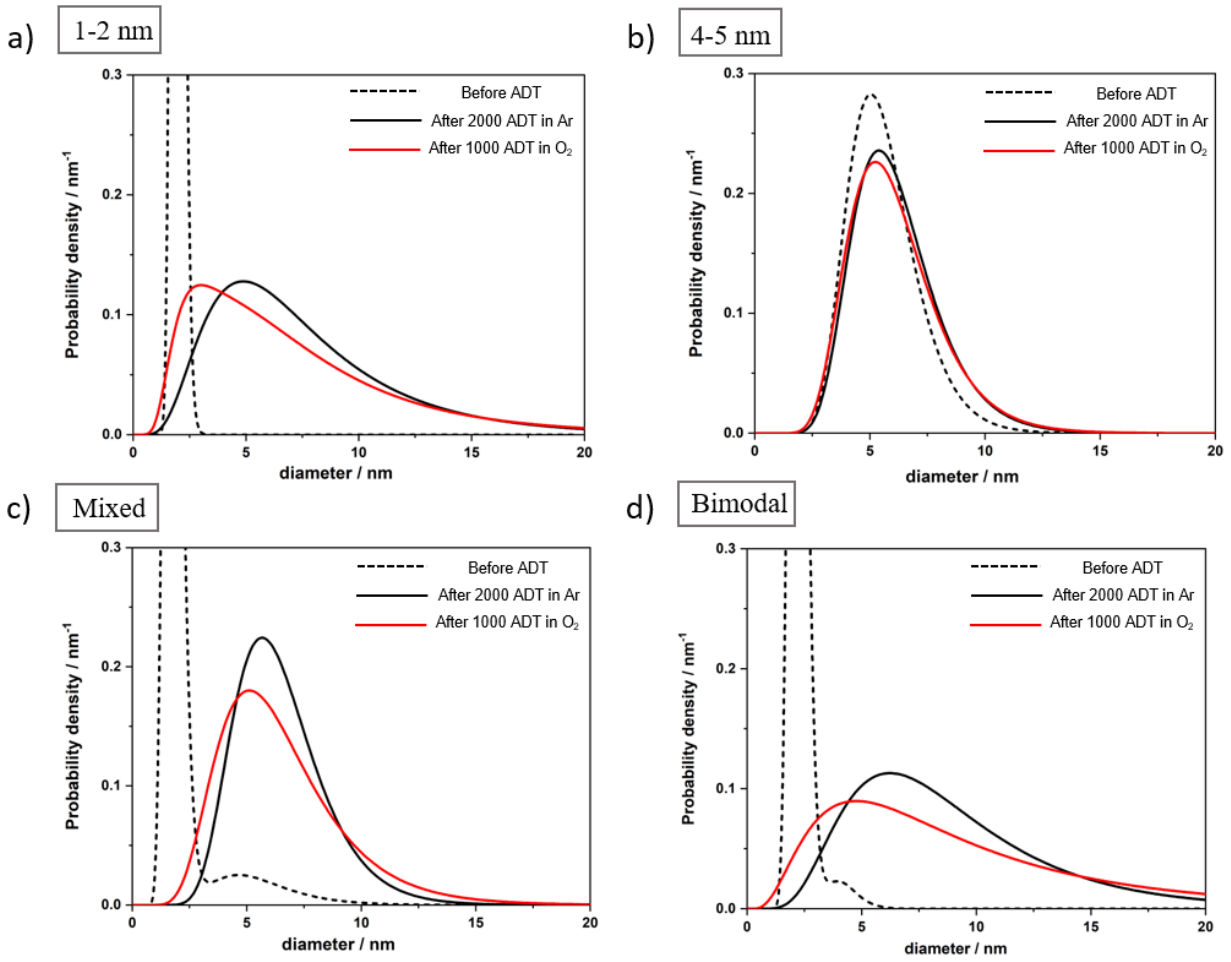

Figure 5. Representative plots of the particle size distribution of the different Pt/C catalysts derived from the SAXS analysis. 1-2 nm (a), 4-5 nm (b), mixed (c), and bimodal (d) Pt/C catalysts before (dashed lines), after 2000 steps of

ADTs in Ar atmosphere (black lines), and after 1000 steps of ADTs in O_2 atmosphere (red lines). All measurements were performed at room temperature.

Comparing the degradation of the 1-2 nm Pt/C and 4-5 nm Pt/C catalysts, the observed changes in particle size distribution upon applying the ADT indicate a significant particle growth for the 1-2 nm Pt/C catalyst while the particle size of the 4-5 nm Pt/C catalyst largely remains unchanged. Furthermore, for the latter no difference in the average particle size is observed between applying the ADT in Ar or O_2 atmosphere, whereas for the 1-2 nm Pt/C catalyst the average particle size is larger after applying 2000 steps in Ar atmosphere as compared to 1000 steps in O_2 atmosphere. The observed increase in particle size for the 1-2 nm Pt/C catalyst indicates electrochemical Ostwald ripening and particle coalescence as the main degradation mechanisms. It is difficult to distinguish if one of the two mechanisms is predominant, but the tail in the size distributions towards larger diameters might point towards particle coalescence[39]. For the 4-5 nm Pt/C the identification of the degradation mechanism is more straight-forward. The negligible increase in particle size distribution cannot explain the significant loss in ECSA, thus indicating particle detachment as the main degradation mechanism[12]. A particle detachment process has also been observed for the degradation of Pt/C in aqueous alkaline media using conventional electrochemical cells by Lafforgue et al.[5]. In their work, the authors showed that Pt NPs catalyze carbon corrosion to CO_2 which results in the local formation of carbonates at the NP support interface (at least in electrolytes compatible with metal carbonates formation, i.e., NaOH, LiOH, KOH, etc.). This mechanism leads to the destruction of the anchoring sites of the NPs and therefore causes the detachment of the NPs from the support. According to their work, the production of carbonates depends on the Pt loading (note that the 4-5 nm Pt/C catalyst has a metal loading of 50.6 wt.% Pt, whereas the 1-2 nm Pt/C catalyst has a metal loading of 19.4 wt.% Pt). It is reported that carbonates are produced above $E = 0.5\ V_{RHE}$ for high Pt weight percent catalysts, but for low Pt weight percent catalysts, this process occurs only above $E = 0.8\ V_{RHE}$. Although in the load-cycling ADT protocol, the applied electrode potential is stepped between 0.6 and 1.0 V_{RHE}, it seems that also in the non-liquid AEM environment particle detachment is enhanced for the 4-5 nm Pt/C catalyst. This observation in itself is however no proof for carbonate formation as cause for particle detachment, because for the 4-5 nm Pt/C catalyst particle detachment was previously also observed in acid electrolyte[12]. Furthermore, in the chosen potential window the formation of CO_2 due to carbon

oxidation should be quite low. Last but not least, if in the GDE environment CO_2 formation would lead to massive particle detachment mechanism as observed in liquid alkaline electrolyte[5], one would expect a more significant decrease in ECSA due to CO stripping experiments. Indeed, it is also reported in a different study by Lafforgue et al. that for a "dry cell" without liquid electrolyte and alkali cations nanoparticle detachment is not favored[40].

With the two other Pt/C catalysts, mixed and bimodal, we intended to investigate the influence of the mesoscopic environment on the degradation mechanism. Both catalysts exhibit two particle size populations as demonstrated by SAXS. What distinguishes the two catalysts is that the mixed catalyst is a mixture of the two catalyst powders of the 1-2 and 4-5 nm Pt/C, whereas for the bimodal catalyst, Pt NPs with a size of around 4 nm were deposited onto the 1-2 Pt/C catalyst. Thus, in the latter case, smaller and larger Pt NPs are immobilized on the same carbon support flakes, whereas in the mixed catalyst they are on separated carbon particles. Indeed, the SAXS data reveal that the two different mesoscopic environments lead to pronounced differences in the particle size distributions upon applying the ADT. For both catalysts after the ADT only a single size population is observed. However, the degraded mixed catalyst exhibits almost exclusively the features of the 4-5 nm Pt/C catalyst (which do not significantly change upon degradation, see above). Only a small increase in particle size is observed which would be consistent with electrochemical Ostwald ripening of the small NPs onto the larger NPs in addition to the particle detachment mechanism. By comparison, the size distribution of the degraded bimodal catalyst exhibits a clear tail towards large NPs. This is also evident comparing the ADT in Ar environment after 1000 and 2000 steps. In contrast to the 4-5 nm Pt/C catalyst a steady increase in the larger particle size is seen, see Figure S3. This observation indicates particle coalescence[41]. As a consequence, the likelihood for electrochemical Ostwald ripening and particle coalescence depends on the mesoscopic environment, with particle coalescence being increased if small and large NPs are immobilized on the same carbon flakes.

Table 3. Average particle sizes derived from the SAXS data analysis.

Average Pt NPs diameter (nm)			
Pt/ C Catalyst	Before ADT	After 2000 steps in Ar	After 1000 steps in O_2
1-2 nm	2.0 ± 0.1	9.0 ± 3.7	5.6 ± 1.9

4-5 nm	5.6 ± 0.9		6.3 ± 1.3	6.4 ± 1.9
Mixed catalyst	1.9 ± 0.2	5.7 ± 1.0	6.7 ± 1.2	6.8 ± 2.0
Bimodal catalyst	2.2 ± 0.2	4.2 ± 0.4	9.9 ± 4.3	11.5 ± 6.2

4. Conclusion

In this work, the application of a GDE setup for investigating the degradation of different Pt/C catalysts under realistic reaction conditions is for the first time demonstrated in an alkaline environment. It is shown that the ECSA loss can be probed by CO stripping without inducing catalyst degradation, which is in contrast to investigations employing conventional electrochemical cells and liquid alkaline electrolyte. As ADT protocol, the popular approach proposed by the FCCJ to simulate load-cycle conditions was applied. It is shown that significant differences in ECSA loss are observed for the different catalysts. The physical characterization of the catalyst layers by SAXS reveals the underlying degradation mechanisms. The results indicate that small Pt NPs and low metal loading tend to degrade via a particle coalescence and Ostwald ripening mechanism. However, it is difficult to disentangle if one of the two is being predominant. By comparison, Pt/C consisting of larger Pt NPs and having higher metal loading degrades mainly via particle detachment; the same mechanism being previously observed in aqueous alkaline electrolyte. However, in contrast to aqueous alkaline electrolyte the results indicate that carbonate formation is not responsible for the observed particle detachment. Comparing the degradation rate[5] and considering the fact that CO stripping measurements do not induce massive degradation, indicates that in a more realistic environment with anion exchange membrane the degradation is less severe. Comparing a mixture of two catalysts with a bimodal catalyst where smaller and larger NPs are immobilized on the same carbon support flakes indicates that particle coalescence is strongly enhanced if small and large NPs are in close vicinity, whereas for the mixed catalyst the small Pt NPs predominantly are subjected to electrochemical Ostwald ripening. The work therefore demonstrates that for an in-depth analysis of degradation mechanisms of fuel cell catalysts such mesoscopic factors need to be considered.

Associated Content

Supporting Information

Additional data and figures including a table of different measurement conditions, two figures concerning the SAXS particle size distribution after 1000 and 2000 ADT in Ar atmosphere and details of the SAXS data for all samples.

Acknowledgments

This work was supported by the Swiss National Science Foundation (SNSF) via the project No. 200021_184742. J.Q. acknowledges the European Union's Horizon 2020 research and innovation program under the Marie Skłodowska-Curie grant agreement No 840523 (CoSolCat).

References

(1) Holdcroft, S. Fuel Cell Catalyst Layers: A Polymer Science Perspective. Chem. Mater. **2014**, 26 (1), 381–393. https://doi.org/10.1021/cm401445h.

(2) Pollet, B. G.; Kocha, S. S.; Staffell, I. Current Status of Automotive Fuel Cells for Sustainable Transport. Curr. Opin. Electrochem. **2019**, 16, 90–95. https://doi.org/10.1016/j.coelec.2019.04.021.

(3) He, Q.; Cairns, E. J. Review—Recent Progress in Electrocatalysts for Oxygen Reduction Suitable for Alkaline Anion Exchange Membrane Fuel Cells. J. Electrochem. Soc. **2015**, 162 (14), F1504–F1539. https://doi.org/10.1149/2.0551514jes.

(4) Gottesfeld, S.; Dekel, D. R.; Page, M.; Bae, C.; Yan, Y.; Zelenay, P.; Kim, Y. S. Anion Exchange Membrane Fuel Cells: Current Status and Remaining Challenges. J. Power Sources **2018**, 375, 170–184. https://doi.org/10.1016/j.jpowsour.2017.08.010.

(5) Lafforgue, C.; Maillard, F.; Martin, V.; Dubau, L.; Chatenet, M. Degradation of Carbon-Supported Platinum-Group-Metal Electrocatalysts in Alkaline Media Studied by in Situ Fourier Transform Infrared Spectroscopy and Identical-Location Transmission Electron Microscopy. ACS Catal. **2019**, 5613–5622. https://doi.org/10.1021/acscatal.9b00439.

(6) Dekel, D. R.; Rasin, I. G.; Brandon, S. Predicting Performance Stability of Anion Exchange Membrane Fuel Cells. J. Power Sources **2019**, 420 (June), 118–123. https://doi.org/10.1016/j.jpowsour.2019.02.069.

(7) Zadick, A.; Dubau, L.; Sergent, N.; Berthomé, G.; Chatenet, M. Huge Instability of Pt/C

Catalysts in Alkaline Medium. ACS Catal. **2015**, 5 (8), 4819–4824. https://doi.org/10.1021/acscatal.5b01037.

(8) Chatenet, M.; Aurousseau, M.; Durand, R.; Andolfatto, F. Silver-Platinum Bimetallic Catalysts for Oxygen Cathodes in Chlor-Alkali Electrolysis: Comparison with Pure Platinum. J. Electrochem. Soc. **2003**, 150 (3), D47. https://doi.org/10.1149/1.1540063.

(9) Roche, I.; Chaînet, E.; Chatenet, M.; Vondrák, J. Durability of Carbon-Supported Manganese Oxide Nanoparticles for the Oxygen Reduction Reaction (ORR) in Alkaline Medium. J. Appl. Electrochem. **2008**, 38 (9), 1195–1201. https://doi.org/10.1007/s10800-008-9537-z.

(10) Dekel, D. R.; Willdorf, S.; Ash, U.; Amar, M.; Pusara, S.; Dhara, S.; Srebnik, S.; Diesendruck, C. E. The Critical Relation between Chemical Stability of Cations and Water in Anion Exchange Membrane Fuel Cells Environment. J. Power Sources **2018**, 375, 351–360. https://doi.org/10.1016/j.jpowsour.2017.08.026.

(11) Dekel, D. R.; Rasin, I. G.; Page, M.; Brandon, S. Steady State and Transient Simulation of Anion Exchange Membrane Fuel Cells. J. Power Sources **2018**, 375, 191–204. https://doi.org/10.1016/j.jpowsour.2017.07.012.

(12) Mayrhofer, K. J. J.; Meier, J. C.; Ashton, S. J.; Wiberg, G. K. H.; Kraus, F.; Hanzlik, M.; Arenz, M. Fuel Cell Catalyst Degradation on the Nanoscale. Electrochem. commun. **2008**, 10 (8), 1144–1147. https://doi.org/10.1016/j.elecom.2008.05.032.

(13) Wiberg, G. K. H.; Fleige, M.; Arenz, M. Gas Diffusion Electrode Setup for Catalyst Testing in Concentrated Phosphoric Acid at Elevated Temperatures. Rev. Sci. Instrum. **2015**, 86 (2). https://doi.org/10.1063/1.4908169.

(14) Inaba, M.; Jensen, A. W.; Sievers, G. W.; Escudero-Escribano, M.; Zana, A.; Arenz, M. Benchmarking High Surface Area Electrocatalysts in a Gas Diffusion Electrode: Measurement of Oxygen Reduction Activities under Realistic Conditions. Energy Environ. Sci. **2018**, 11 (4), 988–994. https://doi.org/10.1039/c8ee00019k.

(15) Sievers, G. W.; Jensen, A. W.; Brüser, V.; Arenz, M.; Escudero-Escribano, M. Sputtered Platinum Thin-Films for Oxygen Reduction in Gas Diffusion Electrodes: A Model System for Studies under Realistic Reaction Conditions. Surfaces **2019**, 2 (2), 336–348. https://doi.org/10.3390/surfaces2020025.

(16) Alinejad, S.; Inaba, M.; Schröder, J.; Du, J.; Quinson, J.; Zana, A.; Arenz, M. Testing Fuel

Cell Catalysts under More Realistic Reaction Conditions: Accelerated Stress Tests in a Gas Diffusion Electrode Setup. J. Phys. Energy **2020**, 2 (2), 024003. https://doi.org/10.1088/2515-7655/ab67e2.

(17) Ohma, A.; Shinohara, K.; Iiyama, A.; Yoshida, T.; Daimaru, A. Membrane and Catalyst Performance Targets for Automotive Fuel Cells by FCCJ Membrane, Catalyst, MEA WG. ECS Trans. **2019**, 41 (1), 775–784. https://doi.org/10.1149/1.3635611.

(18) Ishiguro, N.; Kityakarn, S.; Sekizawa, O.; Uruga, T.; Matsui, H.; Taguchi, M.; Nagasawa, K.; Yokoyama, T.; Tada, M. Kinetics and Mechanism of Redox Processes of Pt/C and Pt3Co/C Cathode Electrocatalysts in a Polymer Electrolyte Fuel Cell during an Accelerated Durability Test. J. Phys. Chem. C **2016**, 120 (35), 19642–19651. https://doi.org/10.1021/acs.jpcc.6b04437.

(19) Speder, J.; Altmann, L.; Roefzaad, M.; Bäumer, M.; Kirkensgaard, J. J. K.; Mortensen, K.; Arenz, M. Pt Based PEMFC Catalysts Prepared from Colloidal Particle Suspensions-a Toolbox for Model Studies. Phys. Chem. Chem. Phys. **2013**, 15 (10), 3602–3608. https://doi.org/10.1039/c3cp50195g.

(20) Speder, J.; Zana, A.; Spanos, I.; Kirkensgaard, J. J. K.; Mortensen, K.; Hanzlik, M.; Arenz, M. Comparative Degradation Study of Carbon Supported Proton Exchange Membrane Fuel Cell Electrocatalysts - The Influence of the Platinum to Carbon Ratio on the Degradation Rate. J. Power Sources **2014**, 261, 14–22. https://doi.org/10.1016/j.jpowsour.2014.03.039.

(21) Nesselberger, M.; Ashton, S.; Meier, J. C.; Katsounaros, I.; Mayrhofer, K. J. J.; Arenz, M. The Particle Size Effect on the Oxygen Reduction Reaction Activity of Pt Catalysts: Influence of Electrolyte and Relation to Single Crystal Models. J. Am. Chem. Soc. **2011**, 133 (43), 17428–17433. https://doi.org/10.1021/ja207016u.

(22) Quinson, J.; Inaba, M.; Neumann, S.; Swane, A. A.; Bucher, J.; Simonsen, S. B.; Theil Kuhn, L.; Kirkensgaard, J. J. K.; Jensen, K. M.; Oezaslan, M.; Kunz, S.; Arenz, M. Investigating Particle Size Effects in Catalysis by Applying a Size-Controlled and Surfactant-Free Synthesis of Colloidal Nanoparticles in Alkaline Ethylene Glycol: Case Study of the Oxygen Reduction Reaction on Pt. ACS Catal. **2018**, 8 (7), 6627–6635. https://doi.org/10.1021/acscatal.8b00694.

(23) Yarlagadda, V.; McKinney, S. E.; Keary, C. L.; Thompson, L.; Zulevi, B.; Kongkanand, A. Preparation of PEMFC Electrodes from Milligram-Amounts of Catalyst Powder. J.

Electrochem. Soc. **2017**, 164 (7), F845–F849. https://doi.org/10.1149/2.1461707jes.

(24) Erlebacher, J.; Snyder, J. Dealloyed Nanoporous Metals for PEM Fuel Cell Catalysis. ECS Trans. **2009**, 25, 603–612.

(25) Wiberg, G. K. H.; Mayrhofer, K. J. J.; Arenz, M. Investigation of the Oxygen Reduction Activity on Silver - A Rotating Disc Electrode Study. Fuel Cells **2010**, 10 (4), 575–581. https://doi.org/10.1002/fuce.200900136.

(26) Inaba, M.; Quinson, J.; Bucher, J. R.; Arenz, M. On the Preparation and Testing of Fuel Cell Catalysts Using the Thin Film Rotating Disk Electrode Method. J. Vis. Exp. **2018**, 2018 (133), 1–10. https://doi.org/10.3791/57105.

(27) Saxsgui v2.15.01. A Graphical User Interface for Visualizing, Transforming and Reducing SAXS Images. http://www.saxsgui.com.

(28) Kajiwara, K.; Hiragi, Y. Chapter 6 Structure Analysis by Small-Angle X-Ray Scattering. In Applications of Synchrotron Radiation to Materials Analysis; Saisho, H., Gohshi, Y. B. T.-A. S. L., Eds.; Elsevier, 1996; Vol. 7, pp 353–404. https://doi.org/https://doi.org/10.1016/S0926-4345(96)80007-1.

(29) Garcia, P. R. A. F.; Prymak, O.; Grasmik, V.; Pappert, K.; Wlysses, W.; Otubo, L.; Epple, M.; Oliveira, C. L. P. An in Situ SAXS Investigation of the Formation of Silver Nanoparticles and Bimetallic Silver–Gold Nanoparticles in Controlled Wet-Chemical Reduction Synthesis. Nanoscale Adv. **2020**, 2 (1), 225–238. https://doi.org/10.1039/C9NA00569B.

(30) Zemb, T.; Lindner, P. Neutron, X-Rays and Light. Scattering Methods Applied to Soft Condensed Matter; 1st Edition, Elsevier, **2002**. ISBN: 9780444511225.

(31) Gasteiger, H. A.; Markovic, N.; Ross, P. N.; Cairns, E. J. CO Electrooxidation on Well-Characterized Pt-Ru Alloys. J. Phys. Chem. **1994**, 98 (2), 617–625. https://doi.org/10.1021/j100053a042.

(32) Schmidt, T. J. Characterization of High-Surface-Area Electrocatalysts Using a Rotating Disk Electrode Configuration. J. Electrochem. Soc. **1998**, 145 (7), 2354. https://doi.org/10.1149/1.1838642.

(33) Zhang, Y.; Chen, S.; Wang, Y.; Ding, W.; Wu, R.; Li, L.; Qi, X.; Wei, Z. Study of the Degradation Mechanisms of Carbon-Supported Platinum Fuel Cells Catalyst via Different Accelerated Stress Test. J. Power Sources **2015**, 273, 62–69.

https://doi.org/10.1016/j.jpowsour.2014.09.012.
(34) Park, Y. C.; Kakinuma, K.; Uchida, M.; Tryk, D. A.; Kamino, T.; Uchida, H.; Watanabe, M. Investigation of the Corrosion of Carbon Supports in Polymer Electrolyte Fuel Cells Using Simulated Start-up/Shutdown Cycling. Electrochim. Acta **2013**, 91, 195–207. https://doi.org/10.1016/j.electacta.2012.12.082.
(35) Ghoshal, S.; Jia, Q.; Bates, M. K.; Li, J.; Xu, C.; Gath, K.; Yang, J.; Waldecker, J.; Che, H.; Liang, W.; Meng, G.; Ma, Z. F.; Mukerjee, S. Tuning Nb-Pt Interactions to Facilitate Fuel Cell Electrocatalysis. ACS Catal. **2017**, 7 (8), 4936–4946. https://doi.org/10.1021/acscatal.7b01061.
(36) Schlögl, K.; Hanzlik, M.; Arenz, M. Comparative IL-TEM Study Concerning the Degradation of Carbon Supported Pt-Based Electrocatalysts. J. Electrochem. Soc. **2012**, 159 (6), B677–B682. https://doi.org/10.1149/2.035206jes.
(37) Schröder, J.; Quinson, J.; Kirkensgaard, J. J. K.; Alinejad, S.; Mints, V. A.; Jensen, K. M. Ø.; Arenz, M. A New Approach to Probe the Degradation of Fuel Catalysts Under Realistic Conditions: Combining Tests in a Gas Diffusion Electrode Setup with Small Angle X-Ray Scattering. **2020**, 1–20. https://doi.org/doi.org/10.26434/chemrxiv.12263804.
(38) Meier, J. C.; Galeano, C.; Katsounaros, I.; Topalov, A. A.; Kostka, A.; Schüth, F.; Mayrhofer, K. J. J. Degradation Mechanisms of Pt/C Fuel Cell Catalysts under Simulated Start-Stop Conditions. ACS Catal. **2012**, 2 (5), 832–843. https://doi.org/10.1021/cs300024h.
(39) Granqvist, C. G.; Buhrman, R. A. Ultrafine Metal Particles. J. Appl. Phys. **1976**, 47 (5), 2200–2219. https://doi.org/10.1063/1.322870.
(40) Lafforgue, C.; Chatenet, M.; Dubau, L.; Dekel, D. R. Accelerated Stress Test of Pt/C Nanoparticles in an Interface with an Anion-Exchange Membrane - An Identical-Location Transmission Electron Microscopy Study. ACS Catal. **2018**, 8 (2), 1278–1286. https://doi.org/10.1021/acscatal.7b04055.
(41) Arenz, M. NanoElectrocatalysis: From Basic Research to Applications in Energy Conversion. Chimia (Aarau). **2018**, 72 (5). https://doi.org/10.2533/chimia.2018.276.